Energy & Environmental Science

Cite this: *Energy Environ. Sci.*, 2012, **5**, 9551

www.rsc.org/ees

PAPER

Semi-transparent polymer solar cells with 6% PCE, 25% average visible transmittance and a color rendering index close to 100 for power generating window applications†

Kung-Shih Chen,[a] José-Francisco Salinas,[ab] Hin-Lap Yip,[a] Lijun Huo,[c] Jianhui Hou[c] and Alex K.-Y. Jen*[a]

Received 22nd June 2012, Accepted 28th August 2012
DOI: 10.1039/c2ee22623e

Inverted semi-transparent organic photovoltaic (OPV) cells with very high device performance, tunable transparency, and extraordinary transparency color perception and rendering properties have been demonstrated for power-generating window applications for buildings and automotives.

Finding economically attractive means to harness the renewable and abundant solar energy on earth has been a vigorously pursued goal toward energy and environmental sustainability. Polymer solar cells have gained appreciable interest for their potential in achieving a low module cost per peak watt through roll-to-roll fabrication processes. They also possess other desirable features such as easy scalability, light weight, and compatibility with flexible substrates and surfaces with complicated contours. Many promising improvements in the performance[1] and stability[2] of polymer solar cells have also been demonstrated in the past few years.

In addition to these encouraging results, the feasibility of realizing semi-transparent device structures shows promise for their use in novel applications. Semi-transparent OPV cells are important building blocks for multijunction or tandem devices,[3] which comprise semitransparent front sub-cells stacked with back sub-cells that have a complementary spectral response which acts to enhance sunlight harnessing and device performance. For this purpose, a major amount of the studies on semi-transparent OPVs have been devoted to the development of transparent electrodes[4–9] as a key step toward the realization of high efficiency tandem organic solar cells.

Moreover, semi-transparent OPV devices have been identified as promising candidates for power-generating window applications because they can be integrated with conventional see-through elements such as building and automobile glasses. Building integration is particularly interesting since buildings have large surface areas for harnessing sunlight and have been recognized as one of the major energy consumers and carbon emitters. Therefore, generating clean energy on site from buildings with integrated low-cost photovoltaics could potentially reduce the expense of energy and mitigate the pollution on an appreciable scale.

However, the current performance of semi-transparent OPVs is much lower than their opaque counterparts, which hinders their applications in power generating windows. For instance, semi-transparent cells based on the most commonly used active materials poly(3-hexylthiophene) (P3HT) and [6,6]-phenyl-C61-butyric acid methyl ester ($PC_{61}BM$) blends show relatively low performance, and their limited spectral absorption results in a strong color bias of the transmitted light.

Though colored windows are useful for aesthetic and decorative purposes, windows with limited chromatic alternations of the light source are generally preferred. They allow a natural color spectrum for environments in which the quality of the illumination is important. The fast development of novel organic photovoltaic materials[10,11] over the past years can be leveraged in realizing high efficiency semi-transparent OPV cells with desirable optical effects. However, systematic study and optimization of the optical properties of semi-transparent OPV for window integration are scarce and have just started to be performed. Ameri *et al.*[12] suggested that semi-transparent OPV cells based on poly[2,6-(4,4-bis-(2-ethylhexyl)-4*H*-cyclopenta[2,1-*b*;3,4-*b*′]dithiophene)-*alt*-4,7-(2,1,3-benzothiadiazole)] (PCPDTBT) and a [6,6]-phenyl-C71-butyric acid methyl ester ($PC_{71}BM$) blend can provide a more natural transparency color perception than the solar cells based on a P3HT:$PC_{71}BM$ blend. Colsmann *et al.*[13] demonstrated that semi-transparent OPV cells based on the blend of $PC_{71}BM$ and poly[(4,4′-bis(2-ethylhexyl)dithieno[3,2-*b*:2′,3′-*d*]silole)-2,6-diyl-*alt*-(2,1,3-benzothiadiazole)-4,7-diyl] (PSBTBT) are suitable candidates for window applications due to the remarkable transparency color perception and color rendering capacity afforded by the transmitted light. However,

[a]*Department of Materials Science and Engineering, University of Washington, Seattle, Washington 98195-2120, USA. E-mail: ajen@u.washington.edu*
[b]*Centro de Investigaciones en Óptica, A.P. 1-948, CP 37000, León, Guanajuato, México. E-mail: franciscost@cio.mx*
[c]*State Key Laboratory of Polymer Physics and Chemistry, Beijing National Laboratory for Molecular Sciences, Institute of Chemistry, Chinese Academy of Sciences, Beijing 100190, China*

† Electronic supplementary information (ESI) available: Material preparation, device fabrication and characterization, optical simulation data and photos of the semi-transparent devices. See DOI: 10.1039/c2ee22623e

further breakthroughs, especially in the performance of semi-transparent OPV cells, rely on the use of more advanced materials and conscious optical engineering.

In this communication, we present high-performance semi-transparent OPVs in the inverted structure comprising blends of PBDTTT-C-T (Fig. 1),[14] which is a low bandgap polymer based on thieno[3,4-*b*]thiophene (TT) and benzo[1,2-*b*:4,5-*b*′]dithiophene (BDT) alternating units with $PC_{71}BM$, as an active material. By tuning the thickness of the reflective metal electrode, the power conversion efficiency (PCE) of the semi-transparent devices ranges from 7.56% to 4.25% with the corresponding transparency ranging from 2% to 36%. The transmitted light of these devices under the air mass 1.5 global (AM1.5G) illumination also exhibits extraordinary transparency color perceptions and rendering capacities, favoring the use of PBDTTT-C-T:$PC_{71}BM$ based semi-transparent solar cells for real-life window applications.

Device fabrication and characterization

The polymer systems based on the BDT and TT alternating units are known to be the most successful donor polymers for organic photovoltaics that have shown excellent PCE.[15–17] Polymer solar cells based on the PBDTTT-C-T:$PC_{71}BM$ bulk-heterojunction (BHJ) in both conventional[14] and inverted[18] structures have been demonstrated to be able to achieve PCEs as high as 7.6% with relatively constant and efficient spectral response across the visible spectrum. This makes them promising absorber materials for window applications.

In this work, we have fabricated semi-transparent inverted devices based on PBDTTT-C-T and $PC_{71}BM$ as active materials to explore their potential for window applications. The inverted architecture is known to have several advantages over the conventional architecture such as improved stability and compatibility with roll-to-roll processes.[19,20] The layout of the device architecture is shown in Fig. 1. The fabrication processes of the semi-transparent OPV cells are described as follows. PBDTTT-C-T (10 mg ml^{-1}) and $PC_{71}BM$ (15 mg ml^{-1}) were dissolved in dichlorobenzene solution with 3 vol.% of 1,8-diiodooctane (DIO) as the solvent additive. Pre-cleaned ITO coated glass substrates (15 Ω $\square^{-1}$) are sequentially spin-coated with ZnO sol–gel, a C_{60} based self-assembled monolayer (C_{60}-SAM, Fig. 1), and the PBDTTT-C-T:$PC_{71}BM$ active layer. Finally, MoO_3 (5 nm) and the Ag anode with variable thickness ($t_{Ag} = 0$–60 nm) are thermally evaporated through patterned masks, defining the nominal area of the devices to be 10.08 mm^2. More detailed descriptions of the device fabrication processes can be found in the ESI.†

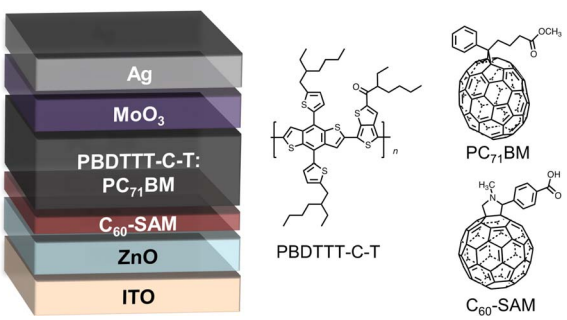

Fig. 1 Device architecture of inverted cells and the chemical structures of the active materials PBDTTT-C-T and $PC_{71}BM$ and the self-assembled molecule C_{60}-SAM.

The inverted semi-transparent OPV cells exhibit a grayish or neutral color appearance due to the complementary and balanced absorption from the PBDTTT-C-T polymer and $PC_{71}BM$ over the visible spectrum. Fig. 2a demonstrates the transmission spectra of the solar cells with varying Ag thickness (open symbols) obtained *via* UV-Vis-NIR spectroscopy. The transmission curve of a Ag electrode free sample ($t_{Ag} = 0$ nm) is also taken for comparison. The average visible transmittance (AVT), or the average of the transmittance of the solar cells in the visible region (370–740 nm), of the semi-transparent devices are presented in Table 1. As the thickness of the reflective Ag electrode varies from 6 nm to 60 nm, the AVT can be tuned accordingly from ~35.9% to ~2.0%, showing the flexibility of transparency management through electrode thickness control. Though the required transparency for windows depends on the working environment, it is generally considered that an AVT of 25% is the benchmark for window applications.[21] In addition, we also show that the AVT of the device without Ag ($t_{Ag} = 0$ nm) is around 50%. Fig. 2b and c demonstrate viewing through the semi-transparent OPV devices of different transparencies.

Device current density–voltage (J–V) measurements were performed under a nitrogen atmosphere with simulated AM1.5

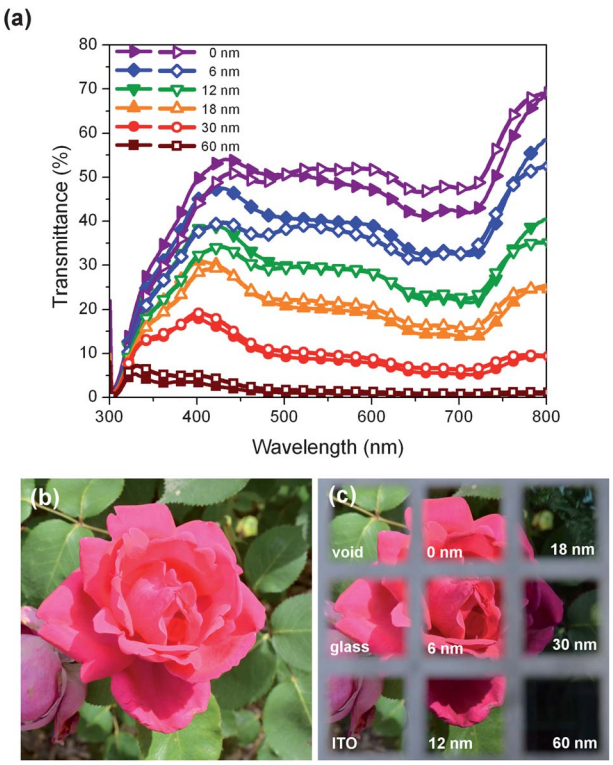

Fig. 2 (a) Transmission spectrum of the semi-transparent OPV devices from optical modeling (closed symbols) and the real devices (open symbols). (b and c) Photographs of a pink rose taken with exactly the same camera settings (shutter, aperture, white balance, *etc.*) on a sunny day. Photograph (c) was taken through semi-transparent devices with the six different Ag thicknesses and blank ITO and glass substrates.

Table 1 Optical properties of the semitransparent devices

Ag thickness (nm)	AVT (%)	HPT (%)	CIE 1931 (x,y)	CCT (K)	$\lvert\Delta_{uv}\rvert$	General CRI
60	2.0	1.4	(0.2650, 0.2617)	15 894	3.90×10^{-3}	94.8
30	10.6	9.5	(0.2917, 0.3010)	8390	3.98×10^{-5}	96.7
18	21.3	21.1	(0.3091, 0.3227)	6764	1.76×10^{-3}	97.3
12	27.9	28.9	(0.3187, 0.3351)	6156	3.34×10^{-3}	96.8
6	35.9	37.3	(0.3225, 0.3442)	5943	6.11×10^{-3}	96.3
0	48.7	51.3	(0.3323, 0.3478)	5507	3.44×10^{-3}	98.0

global solar irradiation at 1 Sun intensity (100 mW cm^{-2}), and the spectral photocurrent was recorded with a lock-in-amplifier under chopped monochromatic illumination in an ambient environment. Fig. 3 and 4 show the J–V curves and the external quantum efficiencies (EQE) of the semi-transparent PBDTTT-C-T:$PC_{71}BM$ devices with different t_{Ag} values, respectively. The series resistance (R_s) and the parallel or shunt resistance (R_p) are estimated from the slopes of the J–V curves at the points where $V = 0$ and $V = V_{oc}$. The sheet resistance ($R_{\square}$) of thin Ag electrodes is characterized using four-point probe measurements on independent samples of Ag films with the same thickness of devices deposited on a 50 nm layer of MoO_3 on glass substrates. Thin Ag films on the MoO_3 substrates have shown $R_{\square}$ values comparable to those of common ITO substrates. A summary of device characteristics can be found in Table 2.

The least transparent semi-transparent OPV device (t_{Ag} = 60 nm, AVT = 2%) shows excellent device performance (J_{sc} = 15.64 mA cm^{-2}, PCE = 7.56%), comparable to the inverted device based on PBDTTT-C-T:$PC_{71}BM$ reported by Li *et al.*[18] High performance OPVs are obtained by optimizing the interfacial property of the devices.[22,23] We found that the modification of the ZnO/active layer interface with the C_{60}-SAM is crucial in our case for optimal device performance. Devices without SAM modification at the ZnO/active layer interface are found to be significantly less efficient; about 20% lower PCE is observed for the device (t_{Ag} = 60 nm) without the C_{60}-SAM modification as shown in Table 2.

The C_{60}-SAM has been shown to improve the electron extraction at the interface.[20,24] The performance of the solar cells is plotted against the AVT and displayed in Fig. 5. It can be observed that the AVT and the device performance oppose each other nearly linearly, which clearly shows the tradeoff between the transparency and photon collection. The performance of several representative semi-transparent OPV devices[9,12,13,25] reported earlier is also displayed in Fig. 5 for comparison. Note the semi-transparent devices based on PBDTTT-C-T:$PC_{71}BM$ show significantly improved performance compared to other semi-transparent OPV devices with similar transparencies. Furthermore, the devices with t_{Ag} = 12 and 18 nm are particularly attractive among the data points since they have presented very practical AVTs between 21% and 28% with excellent PCEs of 6.2% to 5.6%.

Optical perception by the human eye

The visual appearances of the semi-transparent solar cells perceived by human eyes are also the key properties in determining their suitability for applications. Due to the spectrally dependent response of the human eyes, the human perception of color and transparency may vary from the experimental values acquired from the machine. For example, the human perception of transmittance (HPT) of semi-transparent solar cells based on P3HT:$PC_{71}BM$ is distinctly lower than its AVT.[12] Therefore, we analyze the effect of the response of the human eyes by calibrating the transmission spectra of the semi-transparent OPV devices with human eye sensitivity (the y color-matching function) following the procedure reported by Ameri *et al.*[12] The analysis shows only small differences between the HPT and AVT of our semi-transparent OPV devices as summarized in Table 1,

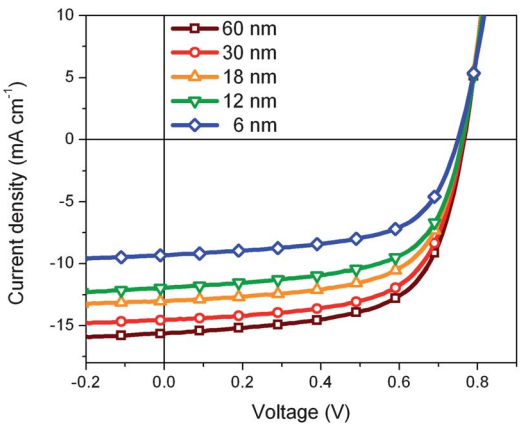

Fig. 3 J–V characteristics of the semitransparent devices with different thicknesses of the silver metal electrode under AM1.5G illumination at 100 mW cm^{-2}.

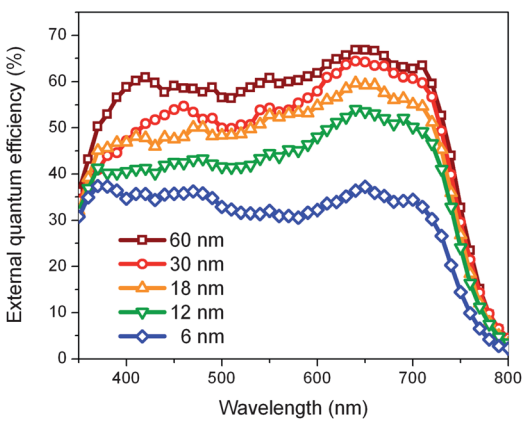

Fig. 4 External quantum efficiency of the semi-transparent OPV devices.

Table 2 Electrical characteristics of the semitransparent solar cells

Ag thickness (nm)	V_{oc} (V)	J_{sc} (mA cm^{-2})	FF	PCE (%)	R_s (Ω cm^2)	R_p (Ω cm^2)	$R_\square$ (Ω □$^{-1}$)
60[a]	0.77 (0.76)[b]	12.13 (12.21)	0.61 (0.57)	5.69 (5.34)	6.4	540.4	1.1
60	0.77 (0.76)	15.64 (15.09)	0.64 (0.63)	7.56 (7.21)	5.4	540.4	1.1
30	0.76 (0.76)	14.54 (14.37)	0.64 (0.62)	7.05 (6.84)	5.7	766.5	3.4
18	0.76 (0.76)	13.01 (12.99)	0.63 (0.62)	6.22 (6.10)	6.4	740.0	8.3
12	0.76 (0.76)	11.94 (11.75)	0.62 (0.62)	5.62 (5.50)	6.4	547.7	12.3
6	0.75 (0.75)	9.33 (9.25)	0.61 (0.61)	4.25 (4.19)	9.2	668.4	8.8×10^8

[a] Device without C_{60}-SAM modification at the ZnO/active layer interface. [b] Numbers in parentheses indicate the average values.

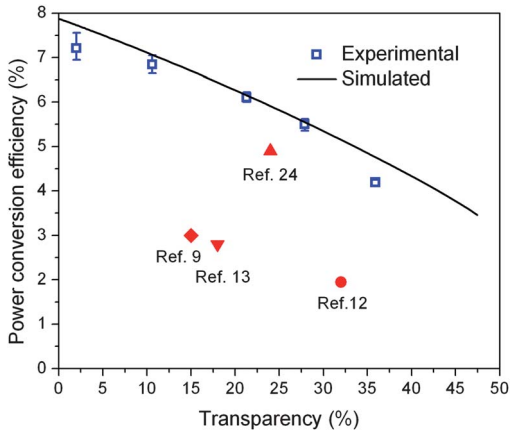

Fig. 5 Experimental (blue markers) and simulated (black line) relationships between the power conversion efficiency and the transparency of the semitransparent devices. Representative semi-transparent OPV devices reported earlier are also displayed for comparison (red markers).

which can be attributed to the balanced absorption of the PBDTTT-C-T:PC_{71}BM blend over the visible range as revealed in the transmission spectra. The transmission spectra and the trivial difference between the AVT and HPT suggest that the semi-transparent OPV cells act similarly to neutral density filters, which is ideal for window applications.

The transparency color perceptions of the semi-transparent OPV devices are depicted using the CIE 1931 chromaticity diagram (xyY), which is specifically designed to represent the colors perceptible to the human eyes. The transmitted light is represented by the product of the AM1.5G solar spectrum and the transmission spectrum of each semi-transparent device, and the corresponding color coordinates CIE 1931 (x,y) are summarized in Table 1. The representation of the color coordinates of the semi-transparent OPV devices are also displayed in the CIE 1931 chromaticity diagram in Fig. 6. The color coordinates of the semi-transparent OPV devices with thin Ag electrodes ($t_{Ag} \leq 30$ nm) are located in the low colorfulness area in the CIE chromaticity diagram, indicating good achromatic or neutral color sensations when looking through the devices under AM1.5G illumination. The transmitted light of the device with $t_{Ag} = 12$ nm and $t_{Ag} = 18$ nm show the color coordinates particularly close to the standard daylight illuminant D65 (x_{D65}, y_{D65}) = (0.3128, 0.3290) at (x_{Ag12}, y_{Ag12}) = (0.3187, 0.3351) and (x_{Ag18}, y_{Ag18}) = (0.3091, 0.3227), respectively, capable of providing extremely high quality illumination with achromatic sensation. The color coordinates move in the direction of the blue corner of the CIE chromaticity diagram as the Ag electrode gets thicker, but overall the color coordinates of the semi-transparent OPV cells suggest transparency color perceptions of neutral colors from the transmitted light with very little color bias caused by the PBDTTT-C-T:PC_{71}BM based semi-transparent solar cells, which is also illustrated in Fig. 2c where the background colors (pink flower and green leaves) were only slightly alternated by the semi-transparent devices.

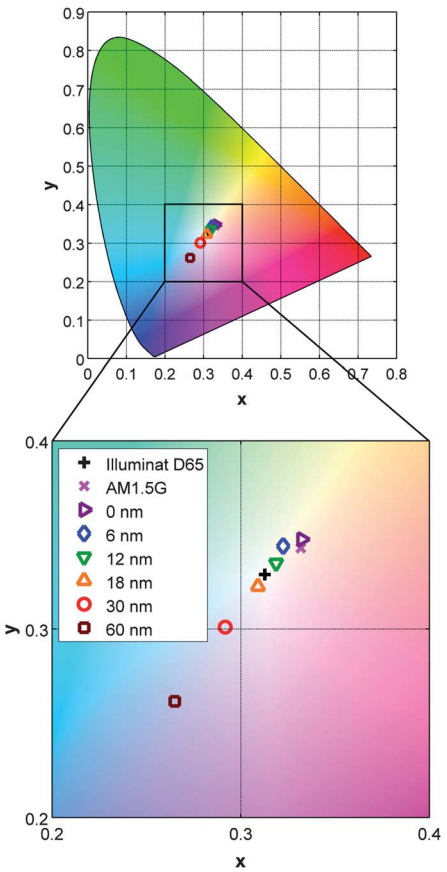

Fig. 6 The representation of the color coordinates of the semi-transparent OPV devices with different thickness of Ag electrode under AM1.5G illumination on the CIE chromaticity diagram xyY (1931) and the enlarged image. The color coordinate representation of D65 standard daylight illuminant and AM1.5G illumination are also presented.

Color rendering capacity

The human visual system is capable of correcting for color deviations caused by varying illumination conditions. This ability is known as color constancy.[26] It has been experimentally determined that the different chromaticities associated with the phases of daylight are close to those of blackbody radiators in the range 4000–25 000 K.[27] Because the color constancy of our vision system under daylight illumination is known to be excellent, blackbody radiators are often referred to in colorimetry as light sources of perfect color rendering capacities. We have demonstrated that the transmitted lights of the semi-transparent OPV devices under AM1.5G illumination are good metamers, or dissimilar spectral distributions that produce the same color sensation, to nearly white light illuminants. However, white light illuminants do not necessarily provide good color rendering capacities. Therefore, we further evaluate the color rendering indices (CRIs) of the transmitted light of the semi-transparent OPV cells.

The trace of the blackbody emission as the function of temperature in a particular color space is known as the Planckian locus or the blackbody locus. When the color coordinate of a light source is considered in the CIE 1960 UCS (uniform color space), the correlated color temperature (CCT) of the light source is defined as the color temperature of the nearest point on the Planckian locus. Note that the CCT is considered meaningful only if the distance between the color coordinate of the light source and the Planckian locus is within ±0.05 as recommended by CIE. The CIE 1931 (x,y) coordinates of the devices are transformed to the UCS CIE 1960 (u, v) color space displayed in Fig. 7. The CCTs of the points and their corresponding distances to the Planckian locus (Δ_{uv}) are calculated from the UCS coordinates and summarized in Table 1. Notably, all points are very close to the Planckian locus with all $|\Delta_{uv}|$ less than 0.05, suggesting the transmitted light of all devices are all still close to those of blackbody radiators.

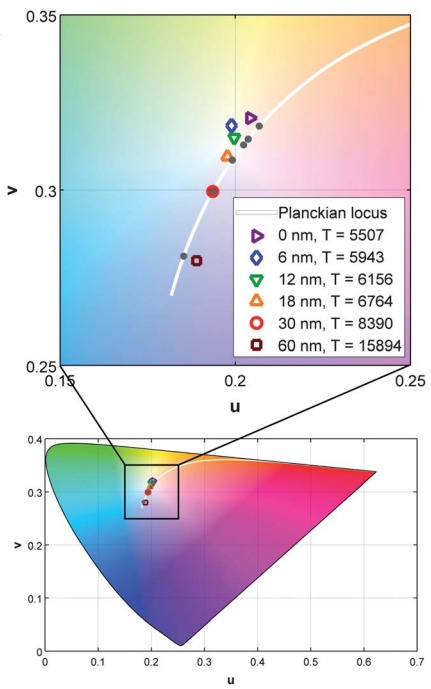

Fig. 7 Planckian locus and the UCS coordinates CIE 1960 (u, v) of the semi-transparent OPV devices. The gray dots represent the nearest Planckian radiators.

The color rendering capacities are analyzed by using the test sample method (TSM).[13] The method compares the color associated in the UCS to 8 standard color samples (TCS01-08) evenly distributed over the complete range of hues when they are illuminated by a probing light, which denote the AM1.5G spectrum folded with the transmission spectrum of any of the semi-transparent OPV cells in this case, and a reference white light source with the same color temperature as the probing light. The choice of the reference white light source is dependent on the CCT.[13] In the case of CCT > 5000 K, a CIE standard illuminant D with the same CCT is used as the reference.

By multiplying the spectra of the color samples with the reference or with the probing light spectra, we have obtained the reflection spectra of the samples, which are further used to calculate their color coordinates in the CIEUVW space and the special CRIs. The mean of the special CRIs is called the general CRI, which represents the color rendering capacity of the sample. By definition, the special and the general CRI can range from 0 to 100, where a higher general CRI represents a better color rendering capacity. The general CRIs of the transmitted light of all semi-transparent OPV devices are listed in Table 1, and the special CRIs are accessible in the ESI.†

The CRIs of all our functional devices are close to 100. To the best of our knowledge, these are the highest general CRI values ever reported for semi-transparent OPV cells. The UCS points of a representative semi-transparent OPV device (t_{Ag} = 12 nm), the nearest Planckian locus point, and the color samples under both the tested and the reference illumination are plotted in Fig. 8. As implied by the excellent general CRIs, the color point corresponding to the semi-transparent OPV cell is almost superimposed on the nearest point on the Planckian locus. Similarly, the corresponding sample color points under both kinds of

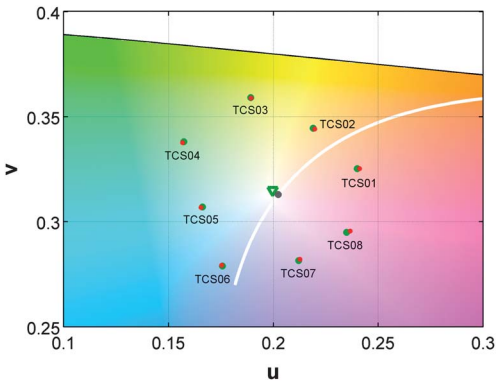

Fig. 8 Determination of the color rendering index of the semi-transparent OPV device with the 12 nm Ag electrode. The central green triangle represents the transmitted light of the PBDTTT-C-T:$PC_{71}BM$ semi-transparent solar cell under AM1.5G illumination. The surrounding green dots correspond to the TCS01–08 illuminated by the transmitted light of the semi-transparent OPV cell under AM1.5G illumination. The red dots represent the TCS01–08 illuminated by the reference Standard illuminant D of CCT = 6156 K.

illuminations are nearly superimposed, clearly demonstrating the exceptional color rendering properties of this system.

Optical simulations

In order to investigate and exploit the full potential of this system, particularly concerning the limitation of transparency imposed on the highest achievable efficiency, optical simulations based on the transfer matrix formalism (TMF)[28] were performed. The optical model comprises 120 nm of ITO, following by 33 nm of sol–gel ZnO, 90 nm of the PBDTTT-C-T:$PC_{71}BM$ (1 : 1.5 w/w) active layer, 5 nm of MoO_3, and finally a Ag layer with variable thickness. Each component is represented by its complex refractive index ($n = \eta + i\kappa$) acquired by variable angle spectroscopic ellipsometry (VASE). The simulations are based on assumptions of planar interfaces and total isotropy for all layers.

A constant energy radiator, *i.e.* illuminant with normalized incident amplitude at all wavelengths, is first applied to the optical model to obtain the electric field distribution inside the solar cells. The electric field intensity profiles of two representative semi-transparent OPV cells (t_{Ag} = 12 nm and 60 nm) can be visualized in Fig. 9. The plots of the electric field distribution of the other devices can be found in the ESI.† The simulations indicate that the distributions of the electric field inside the solar cells are highly wavelength dependent and inhomogeneous as a result of the interference effect.

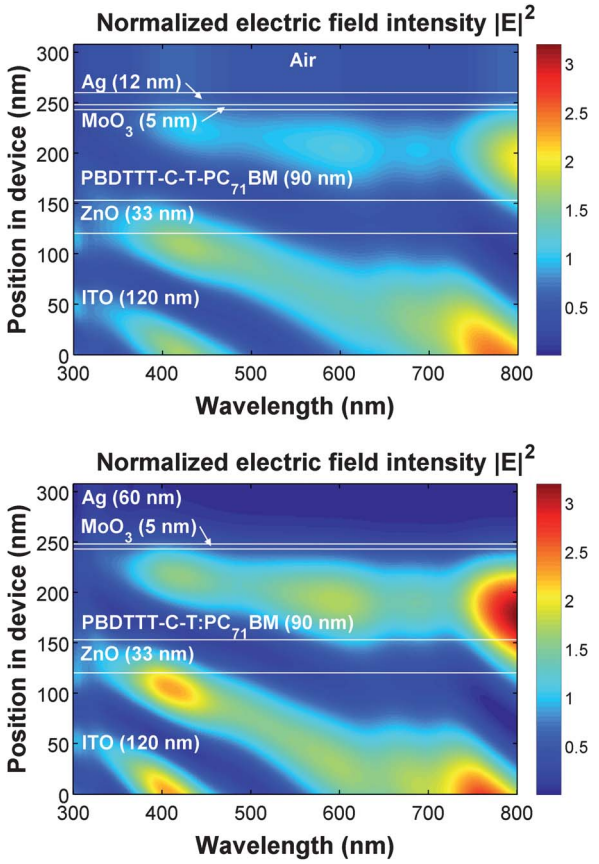

Fig. 9 Simulations for the electric field intensity profile $|E|^2$ in the studied semi-transparent OPV devices with 12 nm (top figure) and 60 nm (bottom figure) Ag electrodes.

Higher intensity of electric field distributed in the device with a thicker Ag electrode is observed as expected due to less transmitted photon loss. From the electric field distributions, simulated transmission curves of the semi-transparent OPV cells are derived and compared with the experimental curves in Fig. 2. We note that the simulated curves are in exceptionally good agreement with the experimental curves, indicating the validity of our model.

Generation of excitons in the active layer is also described as the product of the modulus squared of the electric field obtained from TMF, the AM1.5G spectrum, the real part of the refractive index (η), and the absorption coefficient (α), which is associated to the imaginary part (κ) of the refractive index by $\alpha = 4\pi\kappa/\lambda$ and the factor $c\varepsilon_0/2$, where c is the speed of light in vacuum and ε_0 the permittivity of free space. The devices with 12 nm and 60 nm Ag electrodes are presented in Fig. 10. Again, the plots of the other devices are accessible in the ESI.† It can be observed that the excitons are generated efficiently over the visible regime, which explains the effectiveness of photocurrent generation from the PBDTTT-C-T:$PC_{71}BM$ system.

By integrating the distributed exciton generation rate over the whole active layer, we have also obtained the accumulated exciton generation rate, or the total number of absorbed photons (N_{ph}), in the solar cells. Fig. 11 plots N_{ph} against the continuous change of t_{Ag} (0–100 nm). The trend indicates that N_{ph} is fairly sensitive to the change of t_{Ag} when t_{Ag} is small. N_{ph} starts with a close to linear increment as Ag begins to build up, doubles at $t_{Ag} \sim 25$ nm, and finally reaches a plateau when t_{Ag} is >65 nm. The monotonic and evident enhancement of N_{ph} upon the application of the reflective electrode in the PBDTTT-C-T:$PC_{71}BM$ inverted cell explains the effectiveness of tuning the transparency through control of the thickness of the metal electrode.

Interestingly, the observation is very different from the simulation of semi-transparent inverted P3HT:$PC_{71}BM$ device performed by Ameri *et al.*,[12] where applying a 100 nm opaque reflective electrode to the device only results in relatively mild

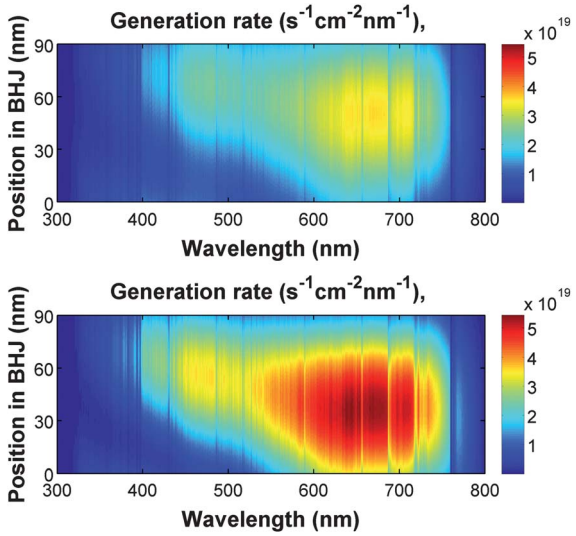

Fig. 10 Simulations of the exciton generation rate in the studied semi-transparent OPV devices with 12 nm (top figure) and 60 nm (bottom figure) Ag electrodes.

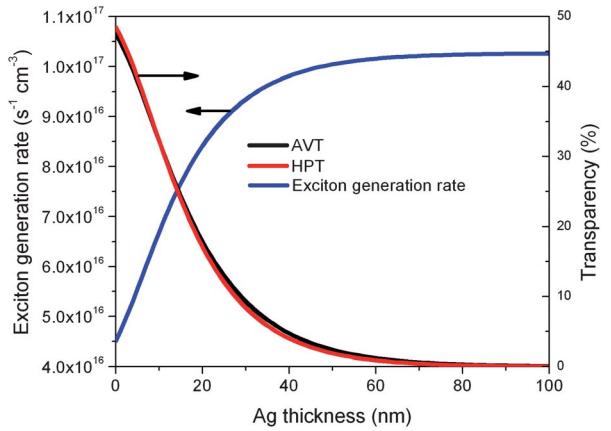

Fig. 11 Dependence of the exciton generation rate on the thickness of the Ag electrode from optical modeling (blue curve). The dependence of the average visible-light transmittance (AVT, black curve) and human perception of transmittance (HPT, red curve) of devices simulated from the optical model at various Ag thicknesses are also revealed.

enhancement of N_{ph}. We attribute the difference between the two systems to the optical effect of the hole-transporting layer. By replacing the 5 nm MoO_3 in the optical model with 100 nm PEDOT:PSS as used in the P3HT:$PC_{71}BM$ inverted solar cell, we observed that the difference of N_{ph} between devices with and without the 100 nm Ag electrode becomes insignificant (data not shown). Fig. 11 also shows the simulations of AVT and HPT at various Ag thicknesses. Again, the figure reveals that HPT is almost identical to AVT at every thickness of Ag.

From the simulation of N_{ph}, we can also estimate the relationship between the highest achievable PCE and transparency by assuming constant internal quantum efficiency (IQE) of 100% at every wavelength, $V_{oc} = 0.76$, and FF = 0.63. The calculation establishes a nearly linear relationship between the highest achievable PCE and the AVT (Fig. 5), which fits the experimental data almost quantitatively. This relationship makes it possible to build devices with predictable performance and transparency. The success of optical simulations in portraying the optical behaviors of the PBDTTT-C-T:$PC_{71}BM$ system indicates their usefulness in designing or engineering future semi-transparent OPV systems.

Conclusions

In conclusion, we have demonstrated high efficiency semi-transparent OPV cells with significantly improved performance compared to other semi-transparent OPV devices of similar transparency. The semi-transparent OPV devices under AM1.5G illumination provide close to white or achromatic transparency color perceptions, especially for the devices with thin Ag electrodes ($t_{Ag} \leq$ 30 nm). The transmitted light from the semi-transparent OPV devices further demonstrates extraordinary transparency color rendering capacities with the highest CRIs (>96) ever reported for semi-transparent OPV devices. These combined advantages suggest that inverted semi-transparent OPV devices based on the PBDTTT-C-T:$PC_{71}BM$ blend can provide high quality transmitted light that is suitable for window applications. We have also established an optical model that accurately portrays the optical behaviors of the semi-transparent OPV systems.

Acknowledgements

This work is supported by the National Science Foundation's NSF-STC program under Grant no. DMR-0120967, the AFOSR (FA9550-09-1-0426), the Office of Naval Research (N00014-11-1-0300), AOARD (FA2386-11-1-4072) and the World Class University (WCU) program through the National Research Foundation of Korea under the Ministry of Education, Science and Technology (R31-10035). A. K.-Y.J. thanks the Boeing-Johnson Foundation for financial support. J. F. Salinas would like to thank to Consejo Nacional de Ciencia y Tecnología (CONACyT) for financial support.

Notes and references

1 M. A. Green, K. Emery, Y. Hishikawa, W. Warta and E. D. Dunlop, *Prog. Photovolt: Res. Appl.*, 2011, **20**, 12–20.
2 M. Jørgensen, K. Norrman, S. Gevorgyan, T. Tromholt, B. Andreasen and F. Krebs, *Adv. Mater.*, 2012, **24**, 580–612.
3 S. Sista, Z. Hong, M.-H. Park, Z. Xu and Y. Yang, *Adv. Mater.*, 2010, **22**, E77–E80.
4 Y. Xia, K. Sun and J. Ouyang, *Energy Environ. Sci.*, 2012, **5**, 5325–5332.
5 W. Gaynor, J.-Y. Lee and P. Peumans, *ACS Nano*, 2010, **4**, 30–34.
6 X. Wang, T. Ishwara, W. Gong, M. Campoy-Quiles, J. Nelson and D. D. C. Bradley, *Adv. Funct. Mater.*, 2012, **22**, 1454–1460.
7 Y. Zhou, H. Cheun, S. Choi, C. Fuentes-Hernandez and B. Kippelen, *Org. Electron.*, 2011, **12**, 827–831.
8 S. K. Hau, H.-L. Yip, J. Zou and A. K.-Y. Jen, *Org. Electron.*, 2009, **10**, 1401–1407.
9 J. Huang, G. Li and Y. Yang, *Adv. Mater.*, 2008, **20**, 415–419.
10 L. Gang, Z. Rui and Y. Yang, *Nat. Photonics*, 2012, **6**, 153–161.
11 Y. J. Cheng, S. H. Yang and C. S. Hsu, *Chem. Rev.*, 2009, **109**, 5868–5923.
12 T. Ameri, G. Dennler, C. Waldauf, H. Azimi, A. Seemann, K. Forberich, J. Hauch, M. Scharber, K. Hingerl and C. J. Brabec, *Adv. Funct. Mater.*, 2010, **20**, 1592–1598.
13 A. Colsmann, A. Puetz, A. Bauer, J. Hanisch, E. Ahlswede and U. Lemmer, *Adv. Energy Mater.*, 2011, **1**, 599–603.
14 L. Huo, S. Zhang, X. Guo, F. Xu, Y. Li and J. Hou, *Angew. Chem., Int. Ed.*, 2011, **50**, 9697–9702.
15 Y. Liang, Z. Xu, J. Xia, S.-T. Tsai, Y. Wu, G. Li, C. Ray and L. Yu, *Adv. Mater.*, 2010, **22**, E135–E138.
16 Y. Liang and L. Yu, *Acc. Chem. Res.*, 2010, **43**, 1227–1263.
17 H.-Y. Chen, J. Hou, S. Zhang, Y. Liang, G. Yang, Y. Yang, L. Yu, Y. Wu and G. Li, *Nat. Photonics*, 2009, **3**, 649–653.
18 X. Li, W. C. H. Choy, L. Huo, F. Xie, W. E. I. Sha, B. Ding, X. Guo, Y. Li, J. Hou, J. You and Y. Yang, *Adv. Mater.*, 2012, **24**, 3046–3052.
19 F. C. Krebs, S. A. Gevorgyan and J. Alstrup, *J. Mater. Chem.*, 2009, **19**, 5442–5451.
20 S. K. Hau, H.-L. Yip, H. Ma and A. K.-Y. Jen, *Appl. Phys. Lett.*, 2008, **93**, 233304.
21 N. Drolet, *Organic Photovoltaic: Efficiency and Lifetime Challenges for Commercial Viability, 2012 MRS Spring Meeting & Exhibit*, San Francisco, CA, Moscone West Convention Center, Marriott Marquis, 2012.
22 H. Ma, H.-L. Yip, F. Huang and A. K.-Y. Jen, *Adv. Funct. Mater.*, 2010, **20**, 1371–1388.
23 H.-L. Yip and A. K.-Y. Jen, *Energy Environ. Sci.*, 2012, **5**, 5994–6011.
24 S. K. Hau, H.-L. Yip, O. Acton, N. Baek, H. Ma and A. K.-Y. Jen, *J. Mater. Chem.*, 2008, **18**, 5113–5119.
25 M. Jan, M. Torben, L. Karl, U. Christian, G. Wolf-Michael, S. Stefan, P. Martin and R. Moritz, *Appl. Phys. Lett.*, 2011, **99**, 043301.
26 J. M. Geusebroek, R. Boomgaard, A. W. M. Smeulders and T. Gevers, *Pattern Recogn. Lett.*, 2003, **24**, 1653–1662.
27 J. Schanda, *Colorimetry Understanding the CIE System*, John Wiley & Sons, USA, 2007, pp. 71–73.
28 L. A. A. Pettersson, L. S. Roman and O. Inganäs, *J. Appl. Phys.*, 1999, **86**, 487–496.